A Hybrid Method For Noise Attenuation In Foggy Images

F. V. N. Silva[1], M. S. Oliveira[1], A. A. Saraiva[1], J. V. M. Sousa[1], N. M. Fonseca Ferreira[2]

[1] Department of Computer Science – State University of Piaui, Piripiri, Piaui, Brazil

[2]Institute of Engineering of Coimbra / Polytechnic Institute of Coimbra, Portugal

Knowledge Engineering and Decision-Support Research Center (GECAD)
of the Institute of Engineering, Polytechnic Institute of Porto

INESC Technology and Science (INESC TEC) – Porto – Portugal.

{viniciunascimento1,marquinhoscamaleao,aratasaraiva,josevigno}@gmail.com
nunomig@isec.pt

Abstract. *The treatment of images captured in situations where there is smoke or fog is a great challenge. Images corrupted by natural effects tend to lose color quality due to the dispersion and absorption of light by the cloudy medium formed by the particles present in the atmospheric environment leaving the image with low visibility of details, harming for example, applications of computer vision. Thus, in this sense, this article presents a hybrid method for attenuation of fog or smoke in digital images, the method is implemented through three stages, and in the first two stages noise filtering is done with two methods already known in the literature, the method of He et al and Meng et al, and in the last step is to make a correction in the intensity of the pixels to improve color quality. After a statistical comparison of the filtering methods in this work using objective metrics MSE, PSNR and SSIM, their visual results are illustrated, proving the improvement of the proposed method.*

Resumo. *O tratamento de imagens captadas em situações onde há fumaça ou neblina é um grande desafio. Imagens corrompidas por efeitos naturais tendem a perder qualidade de cor devido à dispersão e absorção de luz pelo meio turvo formado pelas partículas presentes no ambiente atmosférico deixando a imagem com baixa visibilidade de detalhes, prejudicando, por exemplo, aplicações de visão computacional. Assim, neste sentido, este artigo apresenta um método híbrido de atenuação de névoa ou fumaça em imagens digitais, o método é implementado através de três estágios, e nos dois primeiros estágios a filtragem de ruído é feita com dois métodos já conhecidos na literatura, o método de He et al e Meng et al, e no último passo, um método de correção na intensidade dos pixels para melhorar a qualidade da cor. Após uma comparação estatística dos métodos de filtragem neste trabalho utilizando MEF objetivas, PSNR e SSIM, seus resultados visuais são ilustrados, comprovando a melhoria do método proposto.*

1. Introduction

The treatment of images captured in situations where there is smoke or fog is a great challenge. Images corrupted by natural effects tend to lose color quality due to the dispersion and absorption of light by the cloudy medium formed by the particles present in

the atmospheric environment leaving the image with low visibility of details, harming for example, applications of computer vision.

In this sense a noise removal technique in digital images will benefit many applications of understanding and computational vision of images, such as, classification of images [Shao et al. 2014], aerial images [Woodell et al. 2006], image recovery [Han et al. 2013], video analysis and recognition [Liu and Shao 2013].

In the literature several algorithms have been developed to try to suppress the problem, such as, algorithms based, retinex-based algorithms, contrast elongation algorithms and multi-scale fusion algorithms, among others [Narasimhan and Nayar 2003, Xie et al. 2010, Stark 2000, Ancuti and Ancuti 2013, MAO et al. 2017, Ding et al. 2017, Li et al. 2017, Xu et al. 2017, el Abbadi et al. 2017, Wang et al. 2016, Berman et al. 2016, Bhattacharya et al. 2016, He and Xie 2017, M. S. Oliveira 2018, Saraiva et al. 2018].

Contrast elongation-based algorithms are known to improve the visual effect of the image without the need to reduce the image; however, physics-based techniques are generally capable of achieving better performance compared to others, since the effectiveness of the methods based on physics should be considered a mechanism of degradation where prior knowledge is used for image filtering.

The image filtering search aims to reduce the number of artifacts to represent an image, removing the noise, as much as possible. The ideal is to get the resulting image as close as to the original image. One of the ways to quantify this objective is given by the proximity measurement using the Mean Square Error (MSE) [Talbi et al. 2015] which can be defined mathematically by:

$$MSE = \frac{1}{mn} \sum_{x=0}^{m-1} \sum_{y=0}^{n-1} (I(x,y) - K(x,y))^2 \quad (1)$$

In this equation I represents the original image and K the final image to be compared. The x and y are two matrices of size $M \, xN$, respectively representing the original x-channel and the y-channel to be compared (after filtering).

Another way to compare the quality of the images is the Peak Signal to Noise Ratio (PSNR) what is usually a measure of image quality and can be represented by equation (2) [Fedorov and Rodyhin 2016]. The PSNR ideal of comparison presents an optimum value the higher its is your value.

$$PSNR = 10 \log \frac{MAX^2}{MSE} = 20 \log \frac{MAX}{\sqrt{MSE}} \quad (2)$$

In which, MAX represents the maximum possible value of the pixel in the image and MSE is the value resulting from equation (1).

The main from them is that large distances between pixel intensities do not necessarily mean that the content of the images be dramatically different. It is important to

note that a value of 0 for MSE indicates perfect similarity. A value greater than 1 implies smaller similarity and will continue to grow as the mean difference between pixel intensities increases as well.

In order to sort some of the problems associated with MSE for image comparison, one has the Structural Similarity Index (SSIM). The SSIM is observed by equation (3).

$$SSIM(x,y) = \frac{(2\mu_x\mu_y + c_1)(\sigma_{xy} + c_1)}{(\mu_x^2 + \mu_y^2 + c_1)(\sigma_x^2 + \sigma_y^2 + c_2)} \quad (3)$$

In the equation (3) μ represents the mean, σ symbolizes the standard deviation and σ_{xy} the covariance. And c_1 with c_2 represent constants that avoid the instability of values.

Unlike MSE, the SSIM value can scope from -1 to 1, where 1 indicates perfect likeness.

The essence of SSIM is to model the perceived change in the structural information of the image, while the MSE is actually estimating the perceived errors. There is a subtle difference between the two, but the results can be great.

In addition, the SSIM is used to analyze small sub-samples instead of the entire image as in MSE. The parameters used are the mean of the pixel intensities, the variance of the intensities, together with the covariance. In this way, a more robust approach is obtained capable of explaining the changes in the structure of the image, instead of just the perceived change.

Thus, in this sense, this article presents a hybrid method for attenuation of fog or smoke in digital images, the method is implemented through three steps, in the first two step noise filtering is done and the last step is the one made pixel intensity change to improve color quality. Afterwards, for the quantitative comparison of the filtering methods in this work, the methods of evaluation of objective metrics MSE, PSNR and SSIM were used. Such methods are known as full reference because they consider the original image as a reference.

2. Methodology

The hybrid filtering method implemented in this work is based on the implementations for noise filtering proposed by He et al. [He et al. 2011] and Meng et al. [Meng et al. 2013], where in their methods the authors demonstrated satisfactory results to solve the problem, however, it was noticed that both algorithms leave loopholes to be improved in the quality of the colors of the environment, impelling the research and implementation of the method proposed in this work.

In this way, we verified in the light estimation of the environment of the two methods the opportunity of improvement of results, implementing our algorithm in order to perform the filtering with the two types of estimation.

Initially, prior to the execution of the main algorithm described below, a pre-filtering is performed using as modification the technique of He et al. [He et al. 2011], whereby an image with a smaller amount of noise is generated, increasing the quality

of result after the execution of the main method inspired by the [Meng et al. 2013] technique.

The basic idea of this initial step is to reduce part of the problem so that in the next step it is facilitated the capture of the rest of the noise not filtered by the initial method.

The interpolation model shown below is widely used as a representation of the formation of an image corrupted by the problem, the fog.

$$I(x) = t(x)J(x) + (1 - t(x))A, \tag{4}$$

where $I(x)$ is the observed image, $J(x)$ is the radiation of the scene, A is the atmospheric light and $t(x)$ is the transmission of the scene. The transmission function $t(x)(0 \leq t(x) \leq 1)$ correlates with the depth of the scene. Taking into account that the smoke is normally homogeneous, we can express $t(x)$ by means of:

$$t(x) = e^{-\beta d(x)}, \tag{5}$$

where β is the mean extinction coefficient, and $d(x)$ is the depth of the scene. Then it is necessary to recover the radiation of the scene $J(x)$ of $I(x)$ based on equation 4. This requires estimation of the transmission function $t(x)$ and the global atmospheric light A. Since we estimate $t(x)$ and A, the brightness of the scene can be retrieved by the following equation:

$$J(x) = \frac{I(x) - A}{[max(t(x), s)]^{\delta}} + A, \tag{6}$$

where s is a constant to avoid division by zero, and exponent δ, which has the function of mean extinction coefficient β in equation 5, is used for destructive effects adjustments. However, the destruction of a single image is highly insufficient, since the number of unknowns is much larger than the number of available equations. in this sense we first explore more constraints on the unknowns.

According to equation 1, a pixel corrupted by smoke will be ”pushed” to the global atmospheric light A, as a result it is possible to reverse this process by a linear extrapolation from A to I, by recapturing the clean pixel $J(x)$. The appropriate amount of extrapolation is given by:

$$\frac{1}{t(x)} = \frac{"J(x) - A"}{"I(x) - A"} \tag{7}$$

Consider that the scene radiance of a given image is always bounded, that is,

$$C_0 \leq J(x) \leq C_1, \forall x \square \Omega, \tag{8}$$

where C_0 and C_1 are two constant vectors that are relevant to the given image. Thus, for any x, the extrapolation of $J(x)$ must be located in the radiation cube delimited by C_0 and C_1.

The requirement described in $J(x)$ imposes a limit constraint on $t(x)$. In this sense, suppose that the global atmospheric light A is given. Thus, for each x, it is possible to calculate the corresponding limit constraint point $J_b(x)$. Then a lower bound of $t(x)$ can be determined using equation 7 and equation 8, leading to the following limit restriction at $t(x)$:

$$0 \leq t_b(x) \leq t(x) \leq 1, \tag{9}$$

where $t_b(x)$ is the lower bound of $t(x)$, given by:

$$t_b(x) = min \left[max_{\{c \square \{r,g,b\}\}} \left(\frac{A^c - I^c(x)}{A^c - C_0^c}, \frac{A^c - I^c(x)}{A^c - C_1^c} \right), 1 \right] \tag{10}$$

where I^c, A^c, C_0^c and C_1^c are the color channels of I, A, C_0 and C_1, respectively.

Restriction of the boundary is more fundamental. In most cases, the overall atmospheric light is a bit darker than the brightest pixels in the image. These brightest pixels usually come from some light sources in the scene, for example, the bright sky or the headlights of cars. In these cases, the dark channel prior [MAO et al. 2017] will fail for these pixels, while the proposed limit constraint is still valid.

Usually pixels in a local image patch share a similar depth value. With this assumption, we derive a patch-wise transmission of the constraint limit. On the other hand, this contextual assumption often ceases image stains with abrupt depth leading to significant halo artifacts in the results.

To solve this problem it is possible by adding a weighting function $W(x, y)$ on the constraints, that is,

$$W(x, y)(t(y) - t(x)) \approx 0, \tag{11}$$

where x and y are two neighboring pixels. The weighting function plays a ”switch” of the constraint function between x and y. When $W(x, y) = 0$, the corresponding context-sensitive restriction $t(x)$ between x and y will be canceled.

Noting the fact that depth jumps usually appear at the edges of the image, and that within the local patches pixels of a similar color generally share a similar depth value, it is possible to calculate the color difference of the local pixels to build the weighting function. Here is an example of a weighting function, which is based on the luminance difference of the adjacent pixels:

$$W(x, y) = (|l(x) - l(y)|^{\alpha} + s)^{-1}, \tag{12}$$

where the exponent $\alpha > 0$ controls the sensitivity for difference between pixels, l is the luminance channel of the image $I(x)$ e s is a small constant to avoid division by 0.

The integration of the weighted contextual constraint across the image domain leads to contextual regularization at $t(x)$ below:

$$\int_{x \in \Omega} \int_{y \in \omega_x} W(x,y)\,|t(x) - t(y)|\,dxdy, \tag{13}$$

where Ω is the image domain. In this case, the integral of the L_1 standard is used because this L_1-*norm* is generally more robust to aberrant values than the L_2 *norm*. These atypical values usually arise when wrong contextual constraints are introduced. For example, if two neighboring pixels of a similar color have very different depth values, equation 11 will provide an erroneous constraint.

To reduce the computational cost is given the discrete form equation 13 below:

$$\sum_{i \in I} \sum_{j \in \omega_i} \omega_{ij}\,|t_i - t_j|, \tag{14}$$

where I is the index set of image pixels, ω_{ij} is the discrete versions of $W(x,y)$.

Changing the order of sum of this equation by introducing a set of differential operators, it is possible to rewrite as:

$$\sum_{j \in \omega} \|W_j \circ (D_j \otimes t)\|_1, \tag{15}$$

where ω is an index set, $\circ$ represents the multiplication operator elements, $\otimes$ represents the convolution operator, D_j is a first order differential operator and $W_j\,(j \in \omega)$ is a weighting matrix.

This method uses a minimum filter with a window in motion to filter each color channel for an input image, shortly thereafter the maximum value of each channel is used as an estimate of the component of A.

An optimal transmission function $t(x)$ is found when the objective function illustrated in the equation below is minimized:

$$\frac{\lambda}{2}\|t - \tilde{t}\|_2^2 + \sum_{j \in \omega} \|W \circ (D \otimes t)\|_1, \tag{16}$$

where the first part is the data term that measures the fidelity of $t(x)$, the second part models the contextual constraints of $t(x)$ and λ is used as a regularization parameter for the equilibrium of the two terms.

Then, to optimize this algorithm, an efficient method based on the division of variables is used in Meng et al. [Meng et al. 2013]. The main and simplified idea of

this method is to use several auxiliary variables to construct a sequence of simple sub-problems, whose solutions finally converge to the ideal solution of the original problem.

In order to optimize equation 7 more specifically is presented the following auxiliary variables, denoted by $uj(j\ \bar{\omega})$ and convert equation 7 to a new cost function as shown below:

$$\frac{\lambda}{2}\ t-\hat{t}\ ^{2}{}_{2}+\sum_{j\square\omega}\text{"}W\ _{j}^{\circ}u\ \text{"}_{j}+\frac{\beta}{2}\sum_{j\square\omega}\text{"}u\ -_{j}D\ \square t\text{"}^{2}{}_{2} \tag{17}$$

where β functions as a weight. Thus, as $\beta \longrightarrow \infty$ the solution of equation 8 will converge to that of equation 7.

The minimization of equation 8 to a fixed β is performed with an optimization with respect to u_j and t, so we initially solve for every u_j by fixing t, then we solve each t by correcting u_j until there is convergence. Fortunately, the sub-problems of this process have close-form solutions that can be solved quite efficiently.

Last, but not least, an additional correction is made to the image by means of an intensity correction technique illustrated in the equation 18.

$$FinalImage = \sum_{x=0}^{n-1}\sum_{y=0}^{n-1}(I(x,y)\times v), \tag{18}$$

where I is the resulting image of the previous methods, x and y are the location of the pixel in the coordinates of rows and columns respectively and v represents the value in which it will be used as a multiplier for the current values of each pixel and $FinalImage$ is the resulting image retrieved.

This function is of great importance, since the results of the filtering methods usually produce images recovered with darker pixel intensity, in this way, by using this function it was possible to recover with better fidelity the color quality of the final result.

3. Results

In this section the results obtained are described and compared statistically with other methods by means of the evaluation metrics MSE, PSNR and SSIM respectively. The section describes the results obtained with the use of synthetic images obtained in the frida online repository [J.-P. Tarel and Halmaoui 2012] and the results obtained with the use of images in real environments with addition of fog obtained in the D-Hazy online database [Cosmin Ancuti 2016], in addition images of results of the competing methods and of the proposed method are shown.

Figure 1 illustrates the original image and below the image corrupted by the haze, the original image plays a key role as a reference for the evaluation metrics after the process of filtering the corrupted image.

In the tables 1, 2 and 3, the statistical comparison data of the proposed method and two other competing methods are demonstrated.

Figure 1. Initial images: Original up and with noise below

Table 1. MSE metric result in synthetic images

	MSE		
	He et al.	Meng et al.	Proposed Method
Image a	16.624	16.627	**16.620**
Image b	20.769	20.777	**20.768**
Image c	15.507	15.519	**15.506**
Image d	16.958	16.967	**16.956**
Image e	24.135	24.151	**24.132**
Average	18.798	18.808	**18.796**

Table 1 refers to the amount of MSE for each image after filtering, establishing values. Column 1 shows the name given to each image, and columns 2, 3 and 4 show the respective MSE values obtained for the three methods. The first analysis was done by the MSE metric, presented in all cases the type of method proposed as best, taking into account that the best results are those whose values are smaller. On the other hand, the MSE has the level of trust that is challenged, making it necessary to compare with new forms.

In the table 2 PSNR evaluation is shown, this metric demonstrates in numerical data an approximation of the human perception of reconstruction quality, where not necessarily, but in most cases the highest values represent a better reconstruction of the final image.

When comparing the values resulting from the PSNR, the proposed method presents higher values, if it is more efficient than the other competing methods, it is also

Table 2. PSNR metric result in synthetic images

	PSNR		
	He et al.	Meng et al.	Proposed Method
Image a	5.9233	5.9225	**5.9244**
Image b	4.9565	4.9549	**4.9568**
Image c	6.2254	6.2220	**6.2256**
Image d	5.8369	5.8345	**5.8375**
Image e	4.3042	4.3014	**4.3047**
Average	5.4492	5.4470	**5.4498**

Table 3. SSIM metric result in synthetic images

	SSIM		
	He et al.	Meng et al.	Proposed Method
Image a	0,0026	0.0024	**0.0026**
Image b	0,0031	0.0029	**0.0032**
Image c	**0,0036**	0.0024	0.0032
Image d	0,0042	0.0037	**0.0043**
Image e	0,0035	0.0033	**0.0036**
Average	**0.0034**	0.0029	**0.0034**

Table 4. MSE metric result in real images

	MSE		
	He et al.	Meng et al.	Proposed Method
Image a	26.701	26.737	**26.699**
Image b	9.302	9.305	**9.296**
Image c	21.738	21.740	**21.706**
Image d	16.437	16.465	**16.429**
Image e	19.203	19.228	**19.175**
Average	18.767	18.695	**18.661**

noticed that the mean value of the cases tested in this approach is superior to the others.

Table 3 presents the results of the analysis using a more precise evaluative metric, the SSIM. This metric improves traditional methods, which show inconsistency with human visual perception.

The results presented here, in the tables, prove that the combination of these techniques are very favorable in most of the images, only in one case the value of a competitor was similar to the one proposed in the synthetic image tests.

As a visual example of the results obtained, they are shown in the figure 2. The figure is divided into three columns, the first one illustrates the results obtained by the method of He et al., The second Meng et al., And in the latter is demonstrated the result of the proposed method.

After the tests with synthetic images, the method was used in real images added with fog, in the figure 3 is illustrated the images used, in the upper part the clean images and below each its version with mist.

In the tables 4, 5 and 6 the results of MSE, PSNR and SSIM respectively are shown, where clearly the proposed method is superior to the other competitors, especially in these cases is remarkable the difference between the means of the proposed method and the other methods, in addition it is possible to notice that the colors of the images resulting from the proposed method are more vivid.

In the following figure, the results obtained in the same sequence shown in the results with synthetic images are shown, where in the first column the result is illustrated by He et al. [He et al. 2011], In the second Meng et al. [Meng et al. 2013], and finally the proposed method.

Figure 2. Result images: column(1) He et al., column(2) Meng et al., and column(3) Proposed method.

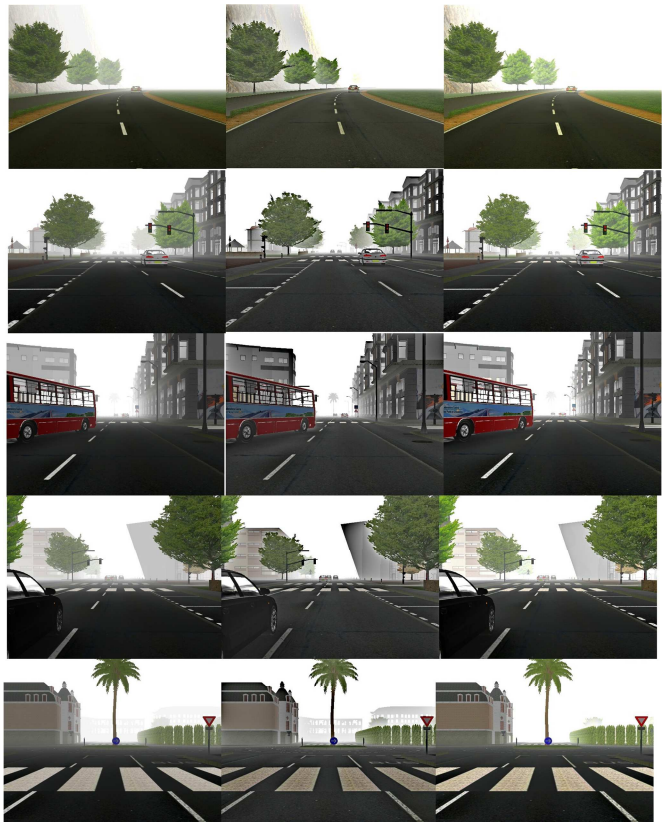

Figure 3. Initial images: Original up and with noise below

Table 5. PSNR metric result in real images

	PSNR		
	He et al.	Meng et al.	Proposed Method
Image a	3.8654	3.8596	**3.8658**
Image b	8.4447	8.4434	**8.4474**
Image c	4.7586	4.7582	**4.7650**
Image d	5.9724	5.9650	**5.9746**
Image e	5.2971	5.2914	**5.3032**
Average	5.6676	5.6635	**5.6712**

Table 6. SSIM metric result in real images

	SSIM		
	He et al.	Meng et al.	Proposed Method
Image a	0.0057	0.0047	**0.0058**
Image b	0.0307	0.0307	**0.0308**
Image c	0.0205	0.0204	**0.0206**
Image d	0.0017	0.0013	**0.0018**
Image e	0.0023	0.0020	**0.0027**
Average	0.0121	0.0118	**0.0123**

Figure 4. Result images: column(1) He et al., column(2) Meng et al., and column(3) Proposed method.

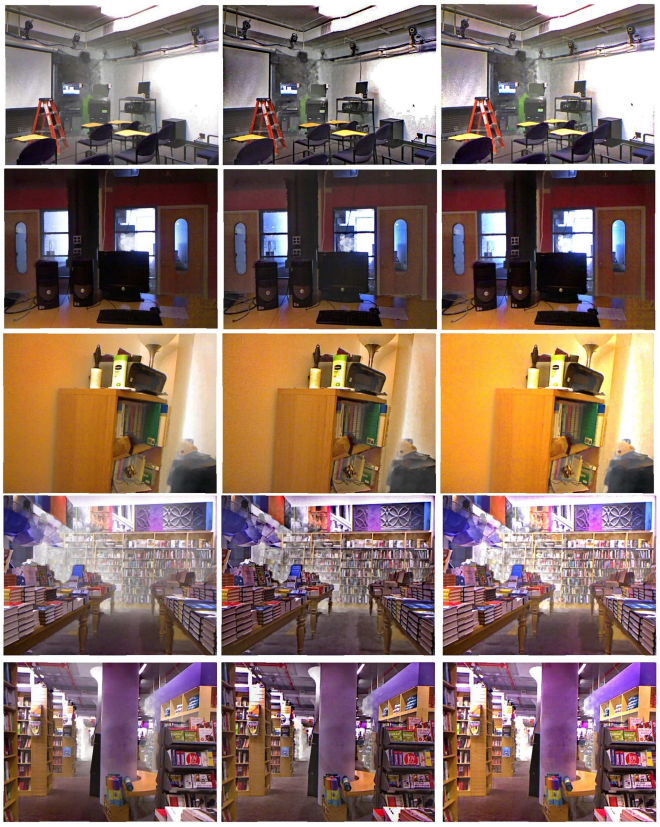

4. Discussion

With the introduction of the method it is evident that there is an improvement of the resolution of the images, making them more interesting for the observation. In the table 1, 2 and 3 it was observed that in all items the method demonstrated the most efficient filtering condition and presented significant statistical results in the filtering of synthetic images obtained from a repository online. Thus, the efficiency of the proposed method in real images was also not different, when compared statistically with the other competing techniques exposed in the tables 4, 5 and 6. In particular, it has been shown that the method is capable of recovering better color quality by providing an increase in the final quality.

5. Conclusion

In this paper, we propose a hybrid method to filter images with natural phenomena based on the capture of smoke and fog by means of the detection of noise density with the use of several mathematical techniques. With the results demonstrated, our method proves to be quite effective to recover details of difficult visibility due to the strong density of noise in some images. For the future, we propose to improve the mathematical method of filtering and improve the speed of processing of results so that we can apply it to real-time capture systems such as aerial images captured by drones or images captured by other mobile robots in a zone of fire.

References

Ancuti, C. O. and Ancuti, C. (2013). Single image dehazing by multi-scale fusion. *IEEE Transactions on Image Processing*, 22(8):3271–3282.

Berman, D., Avidan, S., et al. (2016). Non-local image dehazing. In *Proceedings of the IEEE conference on computer vision and pattern recognition*, pages 1674–1682.

Bhattacharya, S., Gupta, S., and Venkatesh, K. (2016). Dehazing of color image using stochastic enhancement. In *Image Processing (ICIP), 2016 IEEE International Conference on*, pages 2251–2255. IEEE.

Cosmin Ancuti, Codruta O. Ancuti, C. D. V. (2016). D-hazy: A dataset to evaluate quantitatively dehazing algorithms. In *IEEE International Conference on Image Processing (ICIP)*, ICIP'16.

Ding, X., Wang, Y., Zhang, J., and Fu, X. (2017). Underwater image dehaze using scene depth estimation with adaptive color correction. In *OCEANS 2017-Aberdeen*, pages 1–5. IEEE.

el Abbadi, N., Mahdi, H., and Rustum, H. (2017). Single image haze removal via accurate atmosphere light. *International Journal of Applied Engineering Research*, 12(19):9149–9158.

Fedorov, O. and Rodyhin, M. (2016). A referenceless psnr estimator of compressed jpeg images. In *Radioelektronika (RADIOELEKTRONIKA), 2016 26th International Conference*, pages 227–230. IEEE.

Han, J., Ji, X., Hu, X., Zhu, D., Li, K., Jiang, X., Cui, G., Guo, L., and Liu, T. (2013). Representing and retrieving video shots in human-centric brain imaging space. *IEEE Transactions on Image Processing*, 22(7):2723–2736.

He, K., Sun, J., and Tang, X. (2011). Single image haze removal using dark channel prior. *IEEE transactions on pattern analysis and machine intelligence*, 33(12):2341–2353.

He, X. and Xie, C. (2017). Fast image haze-removal algorithm based on mixed filter. In *AOPC 2017: Optical Sensing and Imaging Technology and Applications*, volume 10462, page 1046226. International Society for Optics and Photonics.

J.-P. Tarel, N. Hautière, A. C. D. G. and Halmaoui, H. (2012). Frida (foggy road image database) image database. http://perso.lcpc.fr/tarel.jean-philippe/bdd/frida.html.

Li, C., Zhao, X., Zhang, Z., and Du, S. (2017). Generative adversarial dehaze mapping nets. *Pattern Recognition Letters*.

Liu, L. and Shao, L. (2013). Learning discriminative representations from rgb-d video

data. In *IJCAI*, volume 1, page3.

M. S. Oliveira, F. V. Silva, A. A. S. N. M. F. F. J. V. M. S. (2018). A method for filtering smoke in images.

MAO, X., LI, W., and DING, X. (2017). Single image dehazing algorithm based on sky segmentation. *Journal of Computer Applications*, 10:034.

Meng, G., Wang, Y., Duan, J., Xiang, S., and Pan, C. (2013). Efficient image dehazing with boundary constraint and contextual regularization. In *Computer Vision (ICCV), 2013 IEEE International Conference on*, pages 617–624. IEEE.

Narasimhan, S. G. and Nayar, S. K. (2003). Contrast restoration of weather degraded images. *IEEE transactions on pattern analysis and machine intelligence*, 25(6):713–724.

Saraiva, A., Ferreira, N., and Valente, A. (2018). New bioinspired filter of dicom images.

Shao, L., Liu, L., and Li, X. (2014). Feature learning for image classification via multiobjective genetic programming. *IEEE Transactions on Neural Networks and Learning Systems*, 25(7):1359–1371.

Stark, J. A. (2000). Adaptive image contrast enhancement using generalizations of histogram equalization. *IEEE Transactions on image processing*, 9(5):889–896.

Talbi, M., Ftima, S. B., and Cherif, A. (2015). Image watermarking using data compression. In *Computer Networks and Information Security (WSCNIS), 2015 World Symposium on*, pages 1–9. IEEE.

Wang, Z., Watabe, D., and Cao, J. (2016). Improving visibility of a fast dehazing method. In *World Automation Congress (WAC), 2016*, pages 1–6. IEEE.

Woodell, G., Jobson, D. J., Rahman, Z.-u., and Hines, G. (2006). Advanced image processing of aerial imagery. In *Visual Information Processing XV*, volume 6246, page 62460E. International Society for Optics and Photonics.

Xie, B., Guo, F., and Cai, Z. (2010). Improved single image dehazing using dark channel prior and multi-scale retinex. In *Intelligent System Design and Engineering Application (ISDEA), 2010 International Conference on*, volume 1, pages 848–851. IEEE.

Xu, R.-q., Zhong, S.-h., Tang, G., Wu, J., and Zhu, Y. (2017). Adaptive dehaze method for aerial image processing. In *Pacific-Rim Symposium on Image and Video Technology*, pages 290–301. Springer.